Digest Journal of Nanomaterials and Biostructures Vol. 13, No. 3, July - September 2018, p. 631 - 639

PHOTOCATALYTIC DEGRADATION OF ORGANIC POLLUTANTS WITH PT-$CaFe_2O_4/TiO_2$ COMPOSITE UNDER VISIBLE-LIGHT IRRADIATION

D. P. OJHA[a], H. P. KARKI[a], J. H. SONG[a], H. J. KIM[a,b,*]
[a]*Department of Convergence Technology Engineering, Chonbuk National University, Jeonju 561-756, Republic of Korea*
[b]*Eco-friendly Machine Parts Design Center, Chonbuk National University, Jeonju 561-756, Republic of Korea*

In this study, visible-light active photocatalyst based on TiO_2 was designed using $CaFe_2O_4$ nanoparticle as an effective sensitizer. $CaFe_2O_4$ nanoparticles (CFO) were synthesized by Pechini method using calcium nitrate and iron nitrate. Then, the high crystalline CFO calcined at 800 ^oC was combined with TiO_2 in a simple sol-gel aging. In order to form coupled structure, CFO suspension and TiO_2-precursor solution were mixed in ethanol solution, and then heated at 80 ^oC while vigorously stirring. After 6 hrs, the coupled particles were filtered and dried, followed by calcination at 400 ^oC. The prepared composites were tested for photocatalytic oxidation of Salicylic acid, a model organic compound under visible-light ($\lambda \geq 420$ nm) as monitored by UV-Visible Spectrophotometer. The origin of photoactivity of the heterojunction was found mainly due to the superoxide radical and generation of hydroxyl radical was negligible. The average photo-conversion performance was obtained because of unique energy band matching between CFO and TiO_2.

(Received March 30, 2018; Accepted July 10, 2018)

Keywords: $CaFe_2O_4$, TiO_2, Photocatalysis, Salicylic acid, Visible-light

1. Introduction

Semiconductor-based photocatalysts are valuable materials due to their eco-friendly technological applications in environmental remediation and energy conversion [1-3]. However, some serious drawbacks still restrict practical applications of various semiconductor-based photocatalysts, such as the fast recombination of photogenerated electron−hole pairs and limited visible light response. Thus, it is of great interest for scientists to develop highly efficient visible light photocatalysts to meet the requirements of future practical environmental and energy technologies [4]. Several wide band gap semiconductors such as TiO_2 [5], ZnO [6], WO_3 [7] and $SrTiO_3$ [8] have been studied as photocatalytic material. TiO_2 is the most promising photocatalysts among them because of its suitably placed band position, low cost, chemical stability, and nontoxicity. Likewise, the large band gap (3.2 eV) of TiO_2 only absorbs UV light, which makes up less than 5% of the entire solar spectrum, which is its major limiting factor for practical application [9]. Several strategies for extending visible light absorption with TiO_2 have been investigated and include doping with transition metal or non-metals, deposition of noble metals, surface sensitization, and coupling with another semiconductor. Narrow band gap semiconductors can absorb the visible light that accounts for 40% of the total sunlight, but the efficiency of these photocatalysts alone is relatively low due to fast charge recombination. Fortunately, these semiconductors combined with TiO_2 with a proper band structure can enhance the separation of photo-induced charge by forming well-matched heterojunction or p–n junctions [10].

Therefore, we combined $CaFe_2O_4$ with TiO_2 to construct a heterojunction that can suppress recombination, increase the lifetime of charge carriers, and further effectively improve the photocatalytic activity of semiconductor photocatalysts [3]. We synthesized visible light active $CaFe_2O_4$ nanoparticles and successfully combined them with TiO_2 to obtain an effective electron

*Corresponding author: khanjoo@jbnu.ac.kr

transfer system from the $CaFe_2O_4$ conduction band to the TiO_2 conduction band [11]. Several studies have reported the use $CaFe_2O_4$ as photocatalyst [12-14]. In our present study, we prepared a highly visible light-active photocatalyst that combined the structures of $CaFe_2O_4$ and TiO_2 for the degradation of Salicylic Acid (SA), a phenolic compound, as a model organic pollutant. The photodecomposition of these contaminants is exclusively studied recently by J. Xiao et al [15]. They found the superoxide radical ($\cdot O_2^-$) as a dominant photooxidant. Similarly in our $CaFe_2O_4/TiO_2$ system we studied the origin of the photocatalytic activity with respect to the superoxide radical ($\cdot O_2^-$) and the hydroxyl radical ($\cdot$OH) using electron-hole scavengers. The photodegradation mechanism was proposed.

2. Materials and methods

All chemicals used are of analytical grade and used without further purification.

2.1. Preparation of $CaFe_2O_4$ and $CaFe_2O_4/TiO_2$

$CaFe_2O_4$ nanoparticles (CFO) were synthesized by the Pechini method [16]. For this, 6 mmol of calcium nitrate tetrahydrate with 6 mmol of citric acid and 12 mmol of iron nitrate nonahydrate with 12 mmol of citric acid were dissolved separately in 20 ml of ethanol with magnetic stirring. After 1 hr of continuous stirring, the two solutions were mixed vigorously. Then, 5 ml of distilled water and 2 ml of ethylene glycol were slowly added to the solution. The resulting solution was refluxed at 80 ^oC for 6 h and thermally dried at 100 ^oC. The resulting precipitate was calcined at 800 ^oC for 6 h to obtain pure $CaFe_2O_4$ nanoparticles.

Various $CaFe_2O_4/TiO_2$ heterojunction structures with varying weight percentage of CFO and TiO_2 were prepared (1, 3, 5, 7, 10 and 100 wt% of CFO used). Typically, 0.015 mol of titanium isopropoxide (97%) was gently stirred in a solution containing 30 ml of ethanol, 1 ml of concentrated nitric acid, and 1 ml of water for 30 min. The suitable amount of as-prepared CFO was separately dispersed by ultrasonication in 10 ml of ethanol, and the suspension was added to the Ti-precursor solution. The entire suspension was gently stirred 6 hr and then dried at 90 ^0C for 24 h. Subsequently, the powder was heat treated at 300 ^0C for 3 h for crystallization.

2.2. Characterization

The products were first characterized by X-ray powder diffraction (Rigaku Multiflex diffractometer with monochromatic light-intensity Cu K_α radiation) at a scan rate of 2^o/min (40 kV, 20 mA). UV−vis diffuse reflectance spectroscopy (UV−vis DRS) was used to probe the optical properties. Morphological features of the samples were analyzed using a field-emission scanning electron microscope (FE-SEM, S-7400, Hitachi, Japan), high-resolution transmission electron microscope (HRTEM, JEM-2010F, JEOL, Japan), energy dispersive X-ray spectroscopy (EDX)-mapping. The UV-vis spectra of the MB solutions were recorded on a UV-vis spectrometer (Simatzu UV-1700) at room temperature. The photoluminescence (PL) spectra were measured using a luminescence spectrometer (LS 55; PerkinElmer Inc., USA).

2.3. Evaluation of photoactivity

For the photocatalytic degradation of salicylic acid (SA) in aqueous solution [17], 25 mg of different CFO/TiO_2 composite or other photocatalytic sample was suspended in 25 mL of 50 μM SA aqueous solution with magnetic stirring. Residual pollutant after irradiation with visible light was analyzed from respective characteristic absorption peak at 296 nm detected by UV–vis spectrophotometry. For comparison, bare TiO_2 as prepared and CFO nanoparticles were also tested following same protocol.

3. Results and discussion

P-type Calcium ferrite nanoparticles were synthesized by the thermal decomposition of the respective metal citrates in the presence of ethylene glycol as a surfactant. Figure 1(a) shows XRD

patterns of the as-prepared amorphous $CaFe_2O_4$ samples calcined at different temperatures. All of the diffraction peaks of samples calcined above 800 ^oC were readily categorized as an orthorhombic $CaFe_2O_4$ structure (JCPDS, NO. 65-1333) without any impurity peaks [18]. The crystalline CFO nanoparticles were combined with TiO_2. XRD patterns of several CFO/TiO_2 samples with different CFO weight ratios are shown in Fig. 1(b). The increase of the (302) peak intensity of CFO at 33.57^o corresponded to the increase of CFO component in CFO/TiO_2 composites. Presence of orthorhombic phase only in CFO/TiO_2 composites suggests no appreciable chemical reaction between CFO and TiO_2

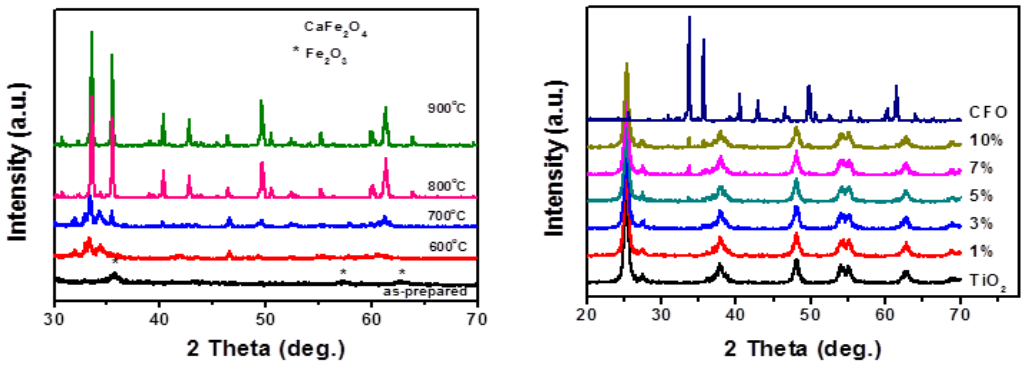

Fig. 1. XRD patterns of the CFO nanoparticles (a) and the CFO/TiO_2 nanocomposites (b) according to various calcination temperature and CFO/TiO_2 ratio, respectively.

Fig. 2 shows TEM and SEM images of CFO and 5/95 CFO/TiO_2 composite. The average diameter of a CFO single particle is ~200 nm Fig. 2(a). Fig. 2(b) represents 5/95 CFO/TiO_2 composite showing the CFO particle at core fully covered with small-sized TiO_2. In order to estimate the coverage of titanium dioxide over the surface of CFO, EDX-mapping images were obtained Fig. 3. The EDX images (Fig. 3(b), 3(d) and 3(e)) show the elements, Ti, Fe and Ca respectively from the 5/95 CFO/TiO_2 composite Fig. (3(a). Consequently, these data clearly indicate that TiO_2 is uniformly distributed and well attached over the entire surface of the CFO nanoparticles.

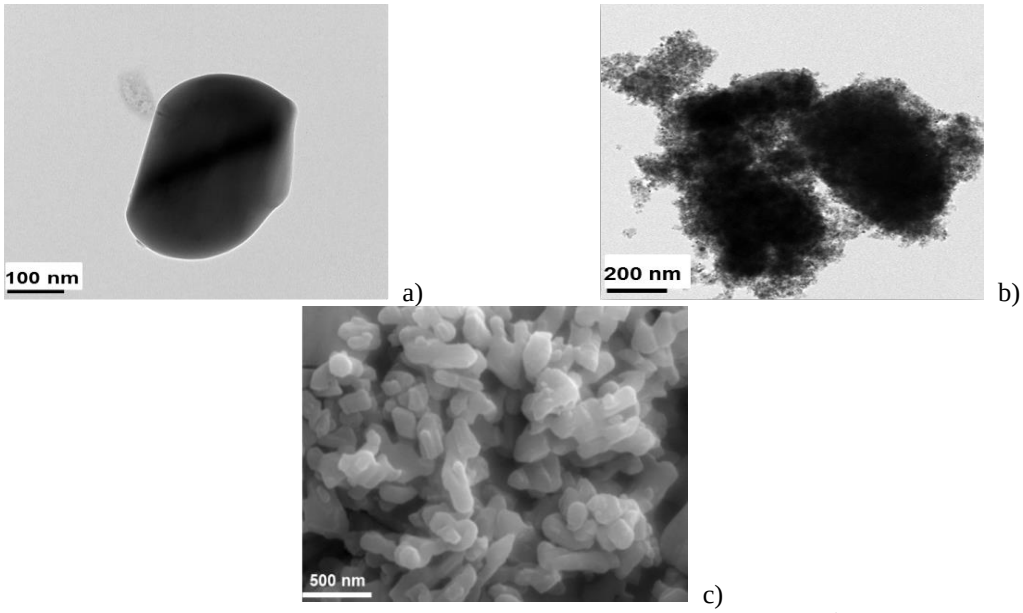

Fig. 2. TEM images for the CFO nanoparticles calcined with 800 ^oC (a) and 5/95 CFO/TiO_2 (b) and SEM image showing the surface of CFO nanoparticle.

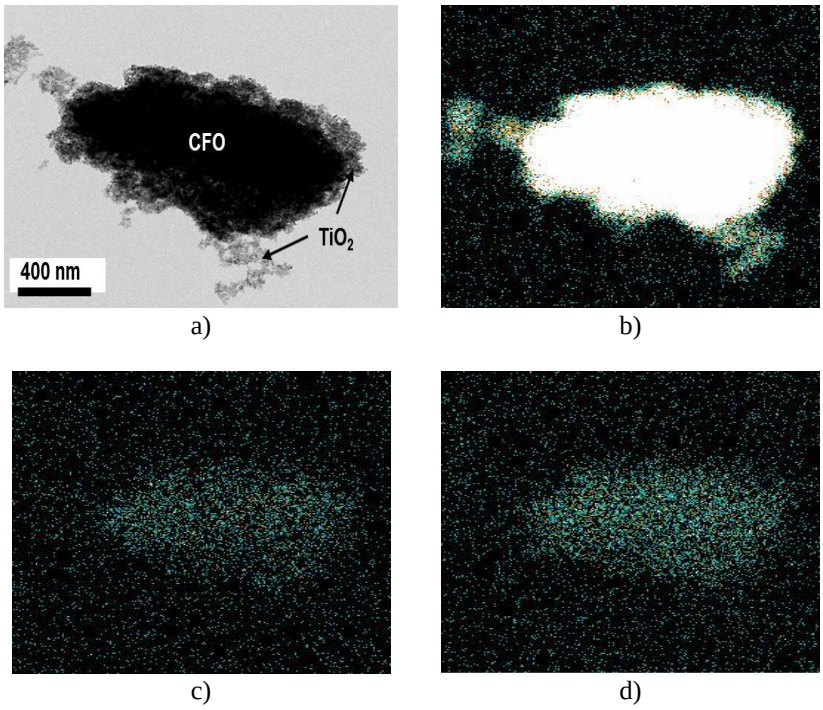

Fig. 3. TEM image of 5/95 CFO/TiO_2 composite (a) and EDX mapping images from (c) showing the elemental composition: (b) Ti, (c) Fe and (f) Ca respectively.

Fig. 4(a) shows UV-visible absorption spectra for CFO, TiO_2, and CFO/TiO_2 composites. Due to its wide band gap, TiO_2 showed low absorption in the visible region, whereas CFO revealed a strong absorption over the entire visible region. As a result, the CFO/TiO_2 composites exhibited significantly higher absorption in the visible region, which was further enhanced with increasing CFO content. The inserted curve in Fig. 4(a) is the Tauc's plot $((\alpha h\nu)^2$ vs. $h\nu)$ [19] of the characteristic absorption edge of CFO, from which the direct band gap of the CFO nanocrystal was estimated to be 1.83 eV. In order to obtain information on the band position between TiO_2 and CFO, Mott-Schottky (M-S) measurements were performed using impedance techniques [20-22]. In Fig. 3(b), M-S plots of electrodes TiO_2 and CFO appear to have characteristics of n-type [23] and p-type [11] semiconductors, respectively. The flat-band potentials, as calculated from the *x* intercepts of the linear region, were found to be -0.56 and 0.96 V vs. Ag/AgCl for TiO_2 and CFO, respectively, which are very close to previously reported values [24].

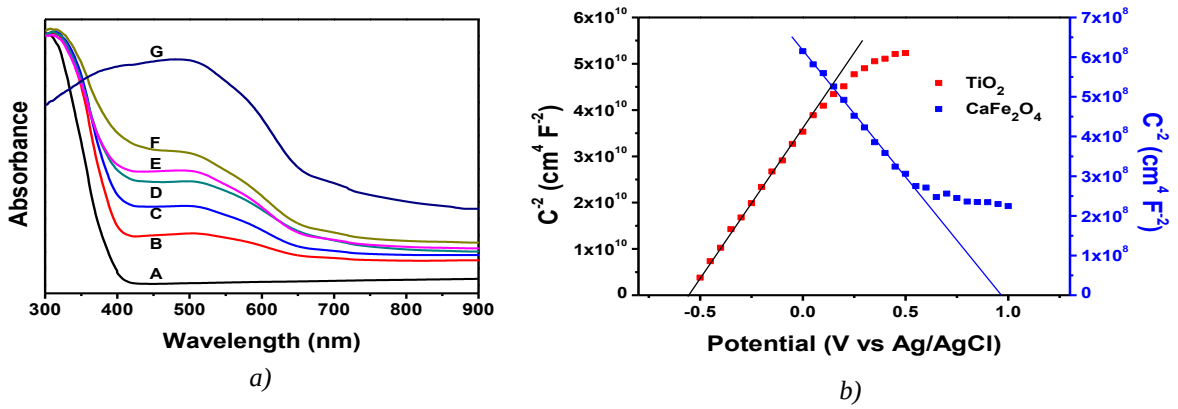

Fig. 4. (a) UV-vis absorption spectra of CFO, TiO_2 and different composed CFO/TiO_2 samples (A: TiO_2, B: 1/99 CFO/TiO_2, C: 3/97 CFO/TiO_2, D: 5/95 CFO/TiO_2, E: 7/93 CFO/TiO_2, F: 10/90 CFO/TiO_2 and G: CFO). The Inserted curve is the Tauc's plot of pure CFO nanoparticle from G. (b) The Mott-schottky plots of pure TiO_2 and CFO ($CaFe_2O_4$).

Fig. 5 shows a plot of the Ti^{+4} 4f peak of the CFO/TiO_2 nanocomposite. The binding energies of each spectrum were referenced to the C 1s core level (284.5 eV), and peak fitting to the spectra was applied using the Gaussian-Lorentzian function after subtraction of Shirley background. For the CFO/TiO_2 sample in Fig 5, the sample is predominantly metallic with the $4f_{7/2}$ appearing at 70.88 eV, but the broad spectrum of Ti^{+4} $4f_{5/2}$ indicates multiple oxidation states including Ti^{2+} and Ti^{+4} [25]. This corresponds to a negative binding energy shift of ca. 0.32 eV with respect to the bulk value of 71.2 eV, which is in agreement with the results of Croy et al. [26] and is close to reported values for similar TiO_2 supported CFO particles [27]. Such negative energy shifts can be explained by charge transfer from the support to the particle due to delocalized electron distributions occurring from oxygen vacancies [28], or small particles with a large number of surface atoms having reduced coordination numbers [29].

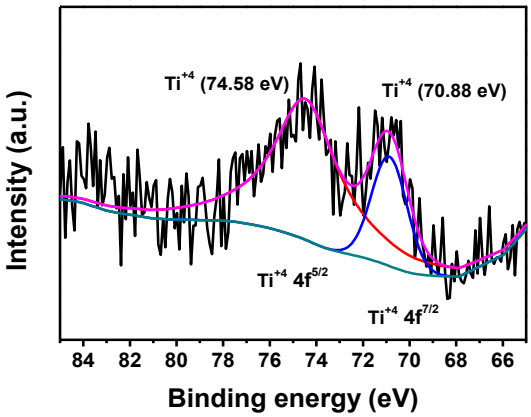

Fig. 5. XPS spectra of Ti^{+4} 4f in CFO/TiO_2 nanocomposites.

The photocatalytic activities of several composites were evaluated by monitoring the decomposition of salicylic acid under visible light irradiation ($\lambda \geq 420$ nm). The decomposition process is considered as pseudo-first order kinetics. Hence, the photocatalytic reaction can simply be described by $-d[c]/dt = k[c]$, where [c] is the concentration of pollutant, and k denotes the degradation rate constant [30]. The graph showing the degradation of SA with TiO_2, CFO, and CFO/TiO_2 composites with different compositions with different time interval is presented in Fig. 6(b) in presence of visible light. 5/95 CFO/TiO_2 decomposed the highest amount of SA, compared to the other composites and the TiO_2 itself. In 3 h, ~63% of the SA was removed with 5/95 CFO/TiO_2, whereas only 41% and 51% was removed with 1% CFO/TiO_2 and 10% CFO/TiO_2 respectively. The determined degradation first order rate constants for decomposition of SA (k) with several photocatalytic samples were calculated. The CFO/TiO_2 composites showed significantly higher photocatalytic activity than bare CFO or a blank TiO_2 sample; among these, the 5/95 CFO/TiO_2 exhibited the highest efficiency: (k) of the 5/95 CFO/TiO_2 was 36.5 and 15.5 fold that of bare CFO and TiO_2, respectively. Compared to the 1% CFO/TiO_2, the efficiency of 5/95 CFO/TiO_2 was 2.5 fold higher. The optimal efficiency was found with the 5/95 CFO/TiO_2 composite. This result suggested that the effective migration of photo-generated electron-hole pair between CFO and TIO_2 in the composites is the main reason behind increased photo-efficiency. However the degradation of SA is relatively slow. This may be because the absence of holes in the VB of TiO_2 that are can generate hydroxyl($^{\bullet}OH$) radical and are widely considered the main active species for the semiconductor photocatalysis [31]. The VB of CFO alone is +1.06 V (Fig. 4) that is way less than the required potential to split water into hydroxyl ($^{\bullet}OH$) radical. Thus we suggested the photodegradation of SA is mainly due to the superoxide ($^{\bullet}O_2^-$) radicals generated at the CB of TiO_2 [15].

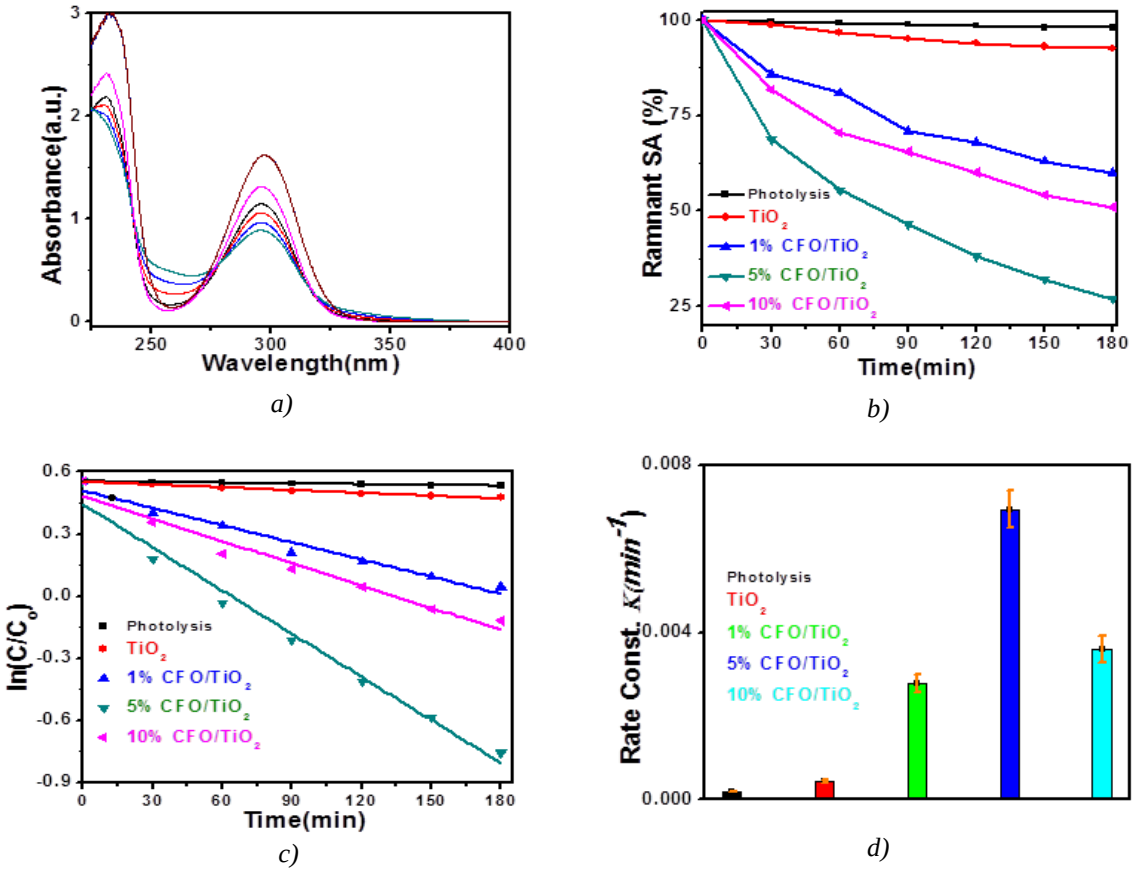

Fig. 6. Photocatalytic activity of several composites: (a) absorption spectra showing SA degradation over 5%CFO/TiO_2; (b) Photodegradation of SA over different samples; (c) first order kinetics of the SA degradation; (d) Degradation rate constant value with error bar.

To clarify the main active species (•OH, $•O_2^-$, h^+) responsible for the photocatalytic degradation of SA by 5/95 CFO/TiO_2, a series of radical trapping experiments with adding various scavengers and PL technique were conducted. During the radical trapping experiments, 1 mmol of isopropanol (IPA, a scavenger of •OH), 1, 4-benzoquinone (p-BQ, a scavenger of $•O_2^-$), 1 mmol of ammonium oxalate (a scavenger of h^+), and 1 μmol of $K_2Cr_2O_7$ (a scavenger of e^-) were used with SA solution under visible light irradiation, respectively. As shown in Fig. 7 (a), the photocatalytic activity of 5/95 CFO/TiO_2 is affected slightly with the addition of IPA. However, the photocatalytic activity of 5/95 CFO/TiO_2 is obviously inhibited when p-BQ or $K_2Cr_2O_7$ is added into the photocatalysis system. Moreover, the photogenerated e^- have the most important influence on the photocatalytic degradation of SA, which is the source of $•O_2-$. Therefore, $•O_2-$ should be the main active species in the photocatalytic degradation of SA by 5/95 CFO/TiO_2. The generation of •OH radicals on the CFO/TiO_2 surface during visible light irradiation was also monitored by photoluminescence spectra [32]. 25 mg of CFO, TiO_2, or CFO/TiO_2 was suspended in 50 mL of an aqueous solution containing 0.01 M NaOH and 1 mM TA. The suspension was stirred in the dark for 30 min and was then irradiated with visible light. Next, 2 mL aliquots of the solution were removed every 1 h for fluorescence measurements [33]. The non-fluorescent terephthalic acid rapidly captures hydroxyl radicals to produce the highly fluorescent 2-hydroxyterephthalic acid. A unique fluorescence peak at 426 nm with 320 nm excitation wavelength light is recorded by spectrofluorometer to ascertain the presence of hydroxyl radical. However, the fluorescence intensity was not increased with irradiation of 30 min (Fig. 7 (b)). This is a clear indication of •OH radical non-formation. Bare TiO_2 suspended in TA solution did not show any appreciable fluorescence peaks upon visible light ($\lambda \geq 422$ nm) irradiation. In addition, bare CFO had a low intensity peak, indicating that photo-generated electron-hole pairs mostly

recombined before the holes could be utilized to form •OH. The potential for generation of $^{\bullet}OH$ is known as +2.27 V (vs NHE at pH 7) (Fig. 4(b)) whereas the valence band position of sensitizer ($CaFe_2O_4$) is only +1.06 V (vs NHE at pH 7) which indicates •OH radical can't be generated. Thus the source of photoactivity was mainly found to be from the conduction band electron.

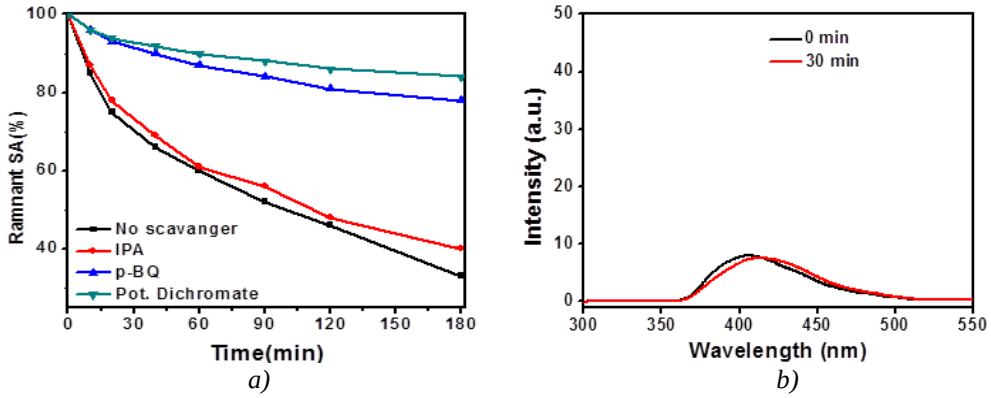

Fig. 7. (a) Radical trapping experiment for the degradation of Salicylic acid (SA) (b) Photoluminescence (PL) spectra of the terephthalic acid solution (5mM) containing 25 mg of 5/95 CFO/TiO_2 composite upon visible irradiation.

The scheme in Fig. 8 outlines the photocatalytic mechanism of the CFO/TiO_2 composite system. Under visible light irradiation, electrons in CFO are excited and photoexcited electrons (e–) and positive holes (h+) are produced in the CFO. The photoexcited electrons are transferred to CB of TiO_2 by charge transfer mechanism. As a result, e– and h+ are separated and trapped by appropriate sites of TiO_2 and CFO to avoid recombination, respectively. The holes at valence band of CFO are used for proton generation. And the interaction of SA molecules with the excited electrons of ($Ti^{3+}$and $^{\cdot}O_2$–) leads to the decomposition of SA. Thus, electrons will be generated in the region neighboring the CB of TiO_2 whereas holes will be formed near the CFO (VB). Thus, the space-charge-separated holes and electrons in TiO_2 will have a greater opportunity to participate in photocatalytic reactions. Since hydroxyl radical is a known powerful oxidizing agent, absence of hydroxyl radical leads to the slow decomposition of SA.

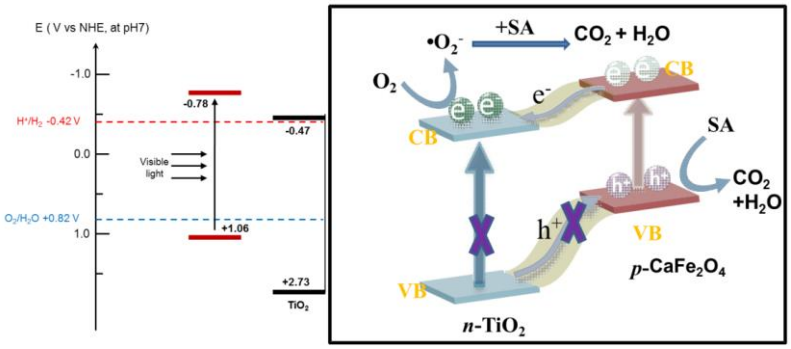

Fig. 8. Diagram for the charge carrier transfer mechanism in the CFO/TiO_2 under visible light irradiation. All potential levels were indicated vs. NHE at pH 7.

It was demonstrated in the present work that the CFO/TiO_2 composite, generating superoxide radial as a major oxidant for the SA and holes on the surface do not take part in the degradation process, provided lower efficiency in the decomposition of SA. This is attributed to the higher VB potential of the CFO from which the hole transfer to the VB of TiO_2 is difficult in CFO/TiO_2 which strongly suggests that the activity of TiO_2 can be enhanced using the sensitizer CFO by activating superoxide radical only.

4. Conclusions

Pure $CaFe_2O_4$ nanoparticles (CFO) with an average diameter of ~200 nm were synthesized by the Pechini method at 800 ^oC. These nanoparticles were combined with TiO_2 to prepare a heterojunction photocatalyst that exhibited higher photocatalytic activity than either bare TiO_2 or CFO due to electron transfer from the CB of CFO to the CB of TiO_2 which finally produces superoxide radical. The generation of electrons on the CB of CFO in the heterojunction upon irradiation with visible light was confirmed by using various scavengers. Since the hole transfer did not occur, hydroxyl radical was not detected. The photocatalytic activity of the heterojunction was thus found mainly due to the superoxide radical participation. This enhancement is due to the generation of electron hole pairs on CFO upon visible light irradiation, which have a longer life due to space-charge separation.

Acknowledgements

This paper was supported by a grant from the Korean Ministry of Education, Science, and Technology (MEST) through the National Research Foundation (NRF) (Project No. 2017-R1C1B2011968). We would also like to thank the staff at the Center for Chonbuk University Research Facility (CURF) for providing the facilities for analysis.

References

[1] H. Kisch, Angewandte Chemie International Edition **52**, 812 (2013).
[2] M. R. Hoffmann, S. T. Martin, W. Choi, D. W. Bahnemann, Chemical Reviews **95**, 69 (1995).
[3] W. Fu, H. Yang, M. Li, M. Li, N. Yang, G. Zou, Materials Letters **59**, 3530 (2005).
[4] P. V. Kamat, Accounts of Chemical Research **50**, 527 (2017).
[5] M. Pelaez, N. T. Nolan, S. C. Pillai, M. K. Seery, P. Falaras, A. G. Kontos, P. S. Dunlop, J. W. Hamilton, J. A. Byrne, K. O'shea, Applied Catalysis B: Environmental **125**, 331 (2012).
[6] K. M. Lee, C. W. Lai, K. S. Ngai, J. C. Juan, Water research **88**, 428 (2016).
[7] J. Kim, C. W. Lee, W. Choi, Environmental Science & Technology **44**, 6849 (2010).
[8] R. Konta, T. Ishii, H. Kato, A. Kudo, The Journal of Physical Chemistry B **108**, 8992 (2004).
[9] G. Wang, X. Xiao, W. Li, Z. Lin, Z. Zhao, C. Chen, C. Wang, Y. Li, X. Huang, L. Miao, Nano Letters **15**, 4692 (2015).
[10] X. Chen, L. Liu, Y. Y. Peter, S. S. Mao, Science **331**, 746 (2011).
[11] S. Ida, K. Yamada, T. Matsunaga, H. Hagiwara, Y. Matsumoto, T. Ishihara, Journal of the American Chemical Society **132**, 17343 (2010).
[12] E. S. Kim, N. Nishimura, G. Magesh, J. Y. Kim, J.-W. Jang, H. Jun, J. Kubota, K. Domen, J. S. Lee, Journal of the American Chemical Society **135**, 5375 (2013).
[13] Z. Liu, Z.-G. Zhao, M. Miyauchi, The Journal of Physical Chemistry C **113**, 17132 (2009).
[14] J. Cao, J. Xing, Y. Zhang, H. Tong, Y. Bi, T. Kako, M. Takeguchi, J. Ye, Langmuir **29**, 3116 (2013) .
[15] J. Xiao, Y. Xie, Q. Han, H. Cao, Y. Wang, F. Nawaz, F. Duan, Journal of Hazardous Materials, **304**, 126 (2016).
[16] R. A. Candeia, M. I. B. Bernardi, E. Longo, I. M. G. Santos, A. G. Souza, Materials Letters **58**, 569 (2004).
[17] D. P. Ojha, M. K. Joshi, H. J. Kim, Ceramics International **43**, 1290 (2017).
[18] N. Sulaiman, M. Ghazali, J. Yunas, A. Rajabi, B. Majlis, M. Razali, Ceramics International, **44**, 46 (2018).
[19] D. B. Buchholz, J. Liu, T. J. Marks, M. Zhang, R. P. H. Chang, ACS Applied Materials & Interfaces **1**, 2147 (2009).
[20] Y. Matsumoto, M. Omae, K. Sugiyama, E. Sato, Journal of Physical Chemistry **91**, 577 (1987).
[21] M. G. Ahmed, T. A. Kandiel, A. Y. Ahmed, I. Kretschmer, F. Rashwan, D. Bahnemann, The Journal of Physical Chemistry C **119**, 5864 (2015).

[22] R. Dom, H. G. Kim, P. H. Borse, ChemistrySelect **2**, 2556 (2017).
[23] W. B. Wu, Z. G. Jin, G. D. Hu, S. J. Bu, Electrochimica Acta **52**, 4804 (2007).
[24] S. Chen, L.-W. Wang, Chemistry of Materials **24**, 3659 (2012).
[25] J. Y. Park, C. Aliaga, J. R. Renzas, H. Lee, G. A. Somorjai, Catalysis Letters **129**, 1 (2009).
[26] J. R. Croy, S. Mostafa, J. Liu, Y. Sohn, H. Heinrich, B. R. Cuenya, Catalysis Letters **119**, 209 (2007).
[27] J. Silvestre-Albero, A. Sepúlveda-Escribano, F. Rodríguez-Reinoso, J. A. Anderson, Journal of Catalysis **223**, 179 (2004).
[28] S. Laursen, S. Linic, Physical Review Letters **97**, 026101 (2006).
[29] O. Björneholm, F. Federmann, F. Fössing, T. Möller, Physical Review Letters **74**, 3017 (1995).
[30] A. Nageswara Rao, B. Sivasankar, V. Sadasivam, Journal of Hazardous Materials **166**, 1357 (2009).
[31] J. Liu, R. Li, Y. Wang, Y. Wang, X. Zhang, C. Fan, Journal of Alloys and Compounds **693**, 543 (2017).
[32] T. Hirakawa, Y. Nosaka, Langmuir **18**, 3247 (2002).
[33] J. Yu, W. Wang, B. Cheng, B.-L. Su, The Journal of Physical Chemistry C **113**, 6743 (2009).